Journal of Clinical and Basic Research
Online ISSN: 2538-3736

Comprehensive in silico prioritization and functional characterization of pathogenic HEXA missense variants in Tay-Sachs disease

Romina Jafari Kalokan [1#], Mohaddeseh Hajmohammadi [1#], Morteza Oladnabi [2,3*]

1. Student Research Committee, Golestan University of Medical Sciences, Gorgan, Iran
2.Gorgan Congenital Malformations Research Center, Jorjani Clinical Sciences Research Institute, Golestan University of Medical Sciences, Gorgan, Iran
3. Ischemic Disorders Research Center, Jorjani Clinical Sciences Research Institute, Golestan University of Medical Sciences, Gorgan, Iran
* Correspondence: Morteza Oladnabi. Ischemic Disorders Research Center, Jorjani Clinical Sciences Research Institute, Golestan University of Medical Sciences, Gorgan, Iran. Tel: +9891044958390; Email: oladnabidozin@yahoo.com
# Both authors contributed equally to the manuscript

Abstract

Background: Tay-Sachs disease (TSD) is a lysosomal storage disorder caused by the accumulation of GM2 gangliosides in neuronal tissues due to reduced or abolished β-hexosaminidase A activity. We conducted a comprehensive computational investigation to prioritize pathogenic missense variants in the HEXA gene and to elucidate their predicted structural and functional consequences through an integrated in silico workflow.

Methods: Complementary bioinformatic tools such as CADD, PolyPhen-2, SIFT, and REVEL were used to predict variant pathogenicity and functional impact. Protein stability was assessed using I-Mutant and MUpro, while STRING, InterPro, and Evolutionary Trace were applied to investigate protein interactions, functional domains, and evolutionary conservation, respectively. Structural analyses were performed using PSIPRED, I-TASSER, ProtScale, and DynaMut2.

Results: Sequential prioritization identified 27 potentially pathogenic variants from an initial set of 124 missense variants. Among the known founder variants, p.Arg170Trp (R170W), frequently observed in the French-Canadian population, met all predefined prioritization criteria and was selected for detailed structural and functional evaluation. The analyses suggested that R170W preserves the overall protein architecture while potentially affecting β-hexosaminidase A function through decreased protein stability, altered molecular interactions, and subtle conformational changes.

Conclusion: Our comprehensive in silico structural and functional analyses provide a practical framework for prioritizing and interpreting pathogenic HEXA variants. The findings suggest that computationally prioritized variants may impair enzyme function through subtle effects on protein stability and structural dynamics while preserving the overall protein fold. This framework may support future efforts in molecular variant interpretation, genetic counseling, and carrier screening, particularly in populations with a high prevalence of Tay–Sachs disease. Further experimental validation is required to confirm these predictions.

Article Type: Research Article

Article History

Received: 19 July 2026
Received in revised form: 12 August 2026
Accepted: 1 September 2026
Available online:
DOI: 10.29252/JCBR.X.X.X

Keywords

Lysosomal Storage Diseases
Protein Stability
Tay-Sachs Disease
Missense Variants
In Silico Analysis

OPEN ACCESS
© The author(s)

Highlights

What is current knowledge?

- Tay-Sachs disease results from HEXA mutations, leading to reduced or absent β-hexosaminidase A activity.
- In silico prediction approaches are widely used to evaluate the pathogenicity and structural consequences of genetic variants.

What is new here?

- Sequential filtering identified 27 candidate pathogenic variants from 124 reported missense variants.
- The French-Canadian founder variant p.Arg170Trp (R170W) was comprehensively characterized, suggesting that its pathogenic effects are primarily due to the destabilization of the protein rather than the disruption of its catalytic core.

Introduction

Tay-Sachs disease (TSD) is an autosomal recessive lysosomal storage disease and one of three conditions characterized by the progressive accumulation of GM2 ganglioside, predominantly in neurons of the central nervous system. This fatal neurodegenerative condition is characterized by β-N-acetylhexosaminidase A deficiency, with clinical symptoms typically appearing when enzyme activity falls below 10% of normal and leading to alterations in the cellular pathways regulating lysosomal lipid catabolism (1-4).

TSD is caused by mutations in the HEXA gene located on chromosome 15q23-q24, which consists of 14 exons within a 35 kb genomic region (Figure 1). This gene encodes the alpha subunit of the heterodimeric beta-hexosaminidase A enzyme (1,5,6). As a result of the deficiency of this enzyme, GM2 is not catabolized and accumulates in the neurons of the brain and spinal cord. This toxic accumulation progressively enlarges neuronal cells and eventually leads to their degeneration and death. Ultimately, TSD manifests with irreversible clinical features such as muscle weakness and hypotonia, progressive loss of motor abilities, dysphagia, speech difficulties, recurrent seizures or muscle spasms, and gradual cognitive and neurological decline (3,5).

Clinically, TSD is classified into infantile, juvenile, and adult-onset forms based on the residual activity of β-hexosaminidase A (3). The acute infantile form typically presents around 6 months of age and progresses rapidly, leading to death by approximately 3 years. Early symptoms include developmental delay, loss of acquired motor skills, muscle weakness, a startle response, and the presence of cherry-red spots in the macula in most cases, due to the accumulation of GM2 in retinal ganglion cells. The juvenile subacute form begins between 3 and 5 years of age and is generally less aggressive than the infantile variant, though it remains fatal by approximately age 15. This form presents with speech disturbances, clumsiness, dysarthria, dysphagia, ataxia, muscle weakness, and is subsequently accompanied by spasticity and seizures. The cherry-red spot on the retina is not consistently observed. The adult chronic form has a delayed clinical presentation, with symptoms that

[DOI: 10.29252/JCBR.X.X.X]

may not appear until adolescence or even the late twenties or early thirties. Life expectancy varies, and due to higher residual enzyme activity, the clinical course is less aggressive. Typically, symptoms include weakness, ataxia, loss of ambulation, dystonia, and a range of psychiatric manifestations (Figure 2). Additionally, a distinct B1 variant of TSD exists, characterized by a phenotype that may overlap with other clinical forms. In this variant, the HEXA protein fails to hydrolyze GM2 ganglioside in vivo due to its different profile. Mutations affecting the active site of HEXA have been observed exclusively in this B1 variant (1,4,7).

TSD is rare in the general population, with an estimated frequency ranging between 1 in 200,000 and 320,000, but it is notably more prevalent among Ashkenazi Jewish individuals (Approximately 1 in 3900 live births without screening) and in French-Canadian, Pennsylvania Dutch, and Irish populations. The implementation of premarital screening has reduced the incidence among Ashkenazi Jewish populations worldwide by about 95% (4,8,9).

To date, over 250 distinct mutations have been identified in the HEXA gene, with the majority (124 variants) being missense/nonsense mutations (10,11) (Figure 3). Mutations primarily impair protein folding, lysosomal trafficking, and α-subunit stability, leading to functional enzyme deficiency (6).

While frameshift, nonsense, and canonical splice-site variants often cause premature termination, mRNA degradation, or truncated, nonfunctional proteins, missense variants can produce diverse clinical phenotypes (12,13). By altering protein structure, stability, or catalytic activity to varying degrees, their pathogenic effects are more difficult to predict and require detailed computational and biophysical analyses (14).

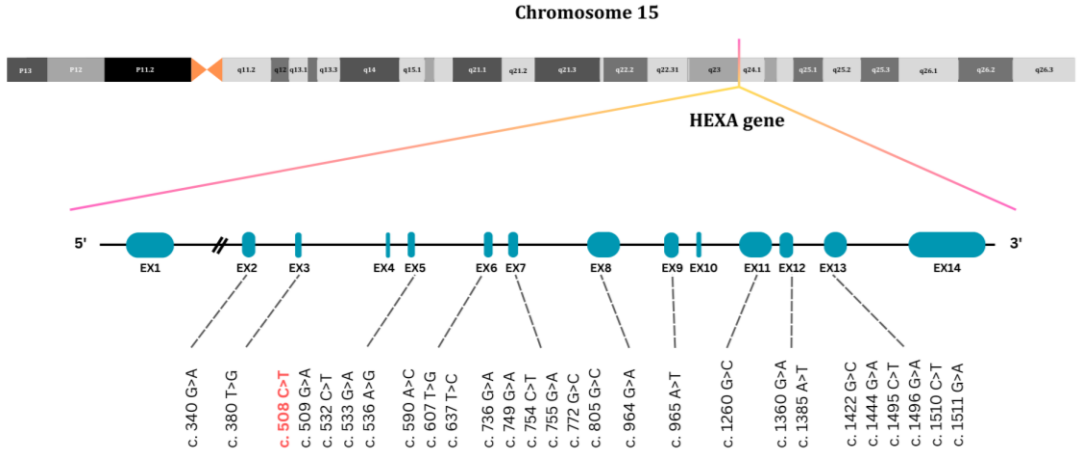


Figure 1. The structure of chromosome 15 and the location of the HEXA gene on 15q23-q24. This gene contains 14 exons. The 27 filtered missense variants analyzed in this study, categorized according to their pathogenicity classification, are shown. The most prevalent pathogenic missense variant in the French-Canadian population is located in exon 5.

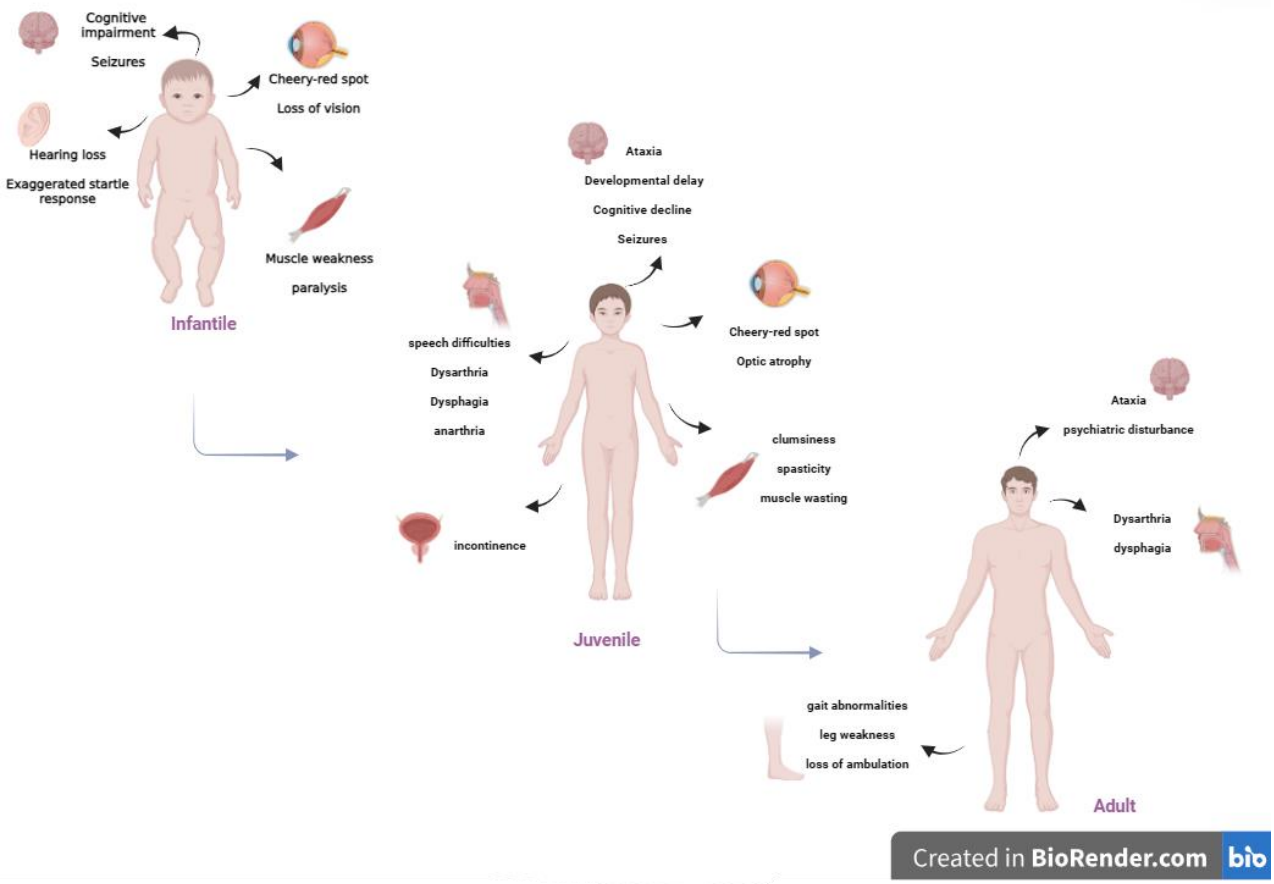


Figure 2. Clinical manifestations of Tay-Sachs disease across the three onset forms: Infantile, Juvenile, and Adult

[DOI: 10.29252/JCBR.X.X.X]



Figure 3. Frequencies of HEXA mutations extracted from the ClinVar database. According to the data, the most frequently reported variants were Uncertain Missense variants (364 variants), followed by pathogenic frameshift variants (63 variants), pathogenic Nonsense variants (47 variants), and pathogenic / likely pathogenic missense variants (45 and 44 variants, respectively). In contrast, the benign and likely benign groups exhibited the lowest report counts.

Despite recent advances in therapeutic strategies for TSD, there are currently no effective approved treatments. Management remains supportive, with drugs and rehabilitative interventions aimed at alleviating neurological symptoms and improving quality of life. However, an ongoing adeno-associated virus (AAV) gene therapy clinical trial has yielded promising results for infantile TSD patients and has transiently arrested disease progression (6,7,15,16). Given the absence of approved therapies, understanding the functional impact of HEXA variants at the molecular level has become increasingly important. Previous in silico studies have provided insights into the molecular basis of TSD, suggesting that alterations affecting lysosomal trafficking and α-β subunit interactions may drive disease severity (7).

The application of bioinformatics tools represents an effective approach for elucidating the pathological mechanisms underlying TSD by analyzing the relationship between molecular alterations in the HEXA protein and disease severity. Identifying pathogenic variants plays a critical role in clinical prognosis, as predictive bioinformatics algorithms can distinguish deleterious mutations from benign polymorphisms. This capability can significantly enhance diagnostic accuracy and inform therapeutic strategies (17).

However, the structural and functional consequences of many candidate HEXA missense variants remain incompletely characterized. While several computational approaches have been employed to predict their pathogenic potential, comprehensive analyses integrating residue-level stability, structural alterations, and functional consequences remain scarce. Addressing this gap is important for improving variant interpretation and strengthening genotype-phenotype correlations in Tay-Sachs disease. Therefore, this study employs a comprehensive in silico framework to prioritize and characterize deleterious missense mutations in the HEXA gene and to identify functionally critical variants relevant to populations with a high prevalence of Tay-Sachs disease.

Methods

Data collection and retrieval

We used the Human Gene Mutation Database (HGMD) to retrieve and categorize reported mutations in the *HEXA* gene. All variants were annotated based on the *HEXA* reference transcript NM_000520.6 and protein accession NP_000511.2. Only missense variants were selected for further *in silico* analysis, as these are directly associated with structural and functional alterations in the *HEXA*-encoded protein. We compiled genetic variants and their associated disease relevance from the NCBI ClinVar (Accessed April 2026; https://clinvar.ncbi.nlm.nih.gov/) database.

Pathogenicity predictio

Based on the ACMG guidelines (https://franklin.genoox.com/clinical-db/), each genetic variant was assigned to one of the five standardized pathogenicity levels: Benign, Likely benign, Uncertain significance, Likely pathogenic, or Pathogenic.

The pathogenicity and functional impact of all identified variants were assessed using multiple bioinformatic tools. The Combined Annotation Dependent Depletion (CADD; https://cadd.gs.washington.edu) tool was utilized to score the deleteriousness of single-nucleotide variants, indels, and multi-nucleotide substitutions. Furthermore, the impact of missense mutations on the structure and function of the protein was predicted using *Polyphen-2* (http://genetics.bwh.harvard.edu/pph2/).

The functional impact of missense substitutions was assessed using SIFT scores, which were retrieved from the Ensembl database (https://www.ensembl.org). Variants resulting in a SIFT score of less than 0.05 were classified as deleterious.

To integrate these predictions, REVEL (18), an ensemble predictor trained on thirteen algorithms (Including MutPred, FATHMM, SIFT, and PolyPhen-2), was used; REVEL scores range from 0 to 1, with higher values suggesting greater pathogenic potential, and variants with a score ≥ 0.5 were classified as potentially pathogenic.

Protein stability analysis

I-Mutant2.0 (https://folding.biofold.org/i-mutant/i-mutant2.0.html) and MUpro (http://mupro.proteomics.ics.uci.edu/) were used to predict protein stability alterations caused by point mutations.

Protein interaction analysis

Protein-protein interaction networks were analyzed using STRING v12.5 (https://string-db.org/). Interactions were predicted based on multiple criteria, including genomic neighborhood, gene fusion, co-expression, experimental data, and database evidence. These interactions are quantified by a score ranging from 0 to 1, with higher values indicating greater confidence in interactions.

Protein sequence classification

We employed InterPro (https://www.ebi.ac.uk/interpro) to classify protein sequences into families. This tool provides comprehensive information on sequence features, predicts the presence of protein domains and important functional sites, and enables the identification of evolutionary relationships among proteins.

Evolutionary trace analysis

Evolutionary conservation of residues was assessed using the Universal Evolutionary Trace (UET) server (wetc package, v.Jan2010; Lichtarge et al.; https://evolution.lichtargelab.org/). This phylogeny-based method enables the identification of critical functional regions and indicates the potential impacts of mutations on protein structure and function (19).

Secondary and tertiary structure prediction

PSIPRED and I-TASSER were employed to perform detailed sequence- and structure-based analyses of the effects of the pathogenic missense variant on the HEXA protein. PSIPRED (https://bioinf.cs.ucl.ac.uk/psipred/) was used to predict secondary structural elements, including α-helices, β-strands, and coil regions, as well as disordered segments, and to generate a two-dimensional structural representation. I-TASSER (https://zhanglab.ccmb.med.umich.edu/I-TASSER/) was then used to model the three-dimensional structure of the HEXA protein.

Hydrophobicity analysis

ProtScale (https://web.expasy.org/protscale/) attributes a numerical value to each amino acid based on properties such as hydrophobicity, hydrophilicity, and secondary structure propensity. In this study, the Kyte-Doolittle scale was applied using a nine-residue sliding window with linear edge weighting (100%) to generate a detailed physicochemical profile of the protein sequence.

Prediction of HEXA protein stability and flexibility upon mutation

DynaMut2 (https://biosig.lab.uq.edu.au/dynamut2/) uses normal-mode approaches to estimate the change in Gibbs free energy (ΔΔG) between wild-type and mutant protein structures. The experimental crystal structure of human β-hexosaminidase A (PDB ID: 2GJX) was retrieved from the Protein Data Bank and used as input. The tool was used to evaluate and visualize the variant's impact on protein stability and conformational dynamics.

[DOI: 10.29252/JCBR.X.X.X]

Results

Pathogenicity and stability prediction of HEXA variants

A total of 124 missense variants of the HEXA gene were retrieved from the public version of the Human Gene Mutation Database (HGMD Public). These variants were initially classified according to the ACMG criteria, and 103 variants categorized as pathogenic or Likely Pathogenic were retained for further analysis. The selected variants were subsequently prioritized using four validated in silico pathogenicity prediction tools, including CADD, PolyPhen-2, SIFT, and REVEL. Each variant was evaluated using predefined thresholds (CADD ≥ 20, PolyPhen-2 > 0.5, SIFT ≤ 0.05, and REVEL ≥ 0.5). Variants meeting all criteria were classified as potentially pathogenic. While all 103 variants passed CADD, PolyPhen-2, and SIFT, combining REVEL (≥0.5) with dual thermodynamic destabilization (I-Mutant/MUpro) yielded 27 prioritized variants for subsequent analyses (As presented in Supplementary Table 1 and Figure 4).

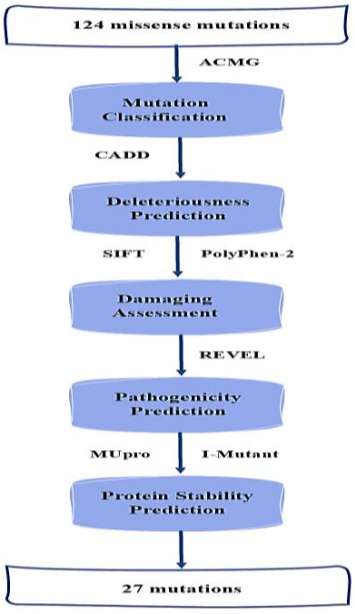


Figure 4. Filtering pipeline. A stepwise filtering strategy was applied to 124 missense variants retrieved from the HGMD database, resulting in the identification of 27 pathogenic variants for further analysis.

Protein interactions of HEXA

STRING-based interaction analysis revealed a network comprising 10 proteins with a confidence score above 0.9, suggesting strong predicted associations among the identified proteins (Figure 5).

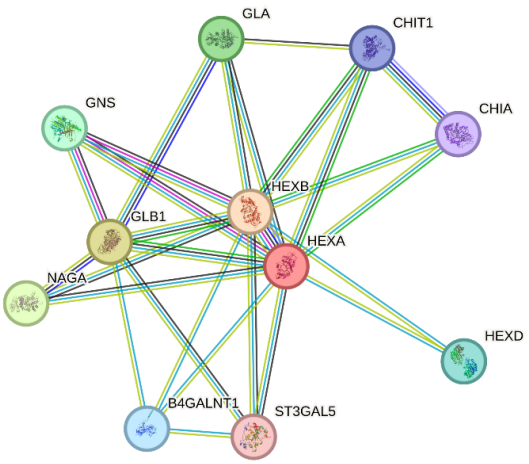


Figure 5. Protein Interaction Network of HEXA. Prediction of HEXA protein interactions using the STRING database revealed that HEXA interacts with proteins involved in lysosomal metabolism, particularly in the catabolism of gangliosides and glycolipids. The strongest predicted interactions were observed with HEXB (Beta-hexosaminidase subunit beta chain A) (0.998), GLB1 (Beta-galactosidase) (0.959), and NAGA (Alpha-N-acetylgalactosaminidase) (0.953).

Structural and functional annotation of the HEXA protein

InterPro annotation classified HEXA as a member of the glycoside hydrolase family 20 (GH20) and the eukaryotic β-hexosaminidase subfamily, featuring an N-terminal HEX domain essential for structural integrity and β-subunit assembly, and a central GH20 catalytic domain responsible for substrate binding and enzymatic catalysis. Mapping the 27 prioritized variants onto the HEXA functional domains showed predominant localization within the catalytic domain (21 variants), with additional variants distributed across the N-terminal and C-terminal regions (Supplementary Table 1). Furthermore, all 27 prioritized variants exhibited consistent predicted destabilizing effects ($\Delta\Delta G < 0$) across both I-Mutant and MUpro algorithms (Supplementary Table 1).

Conservation of HEXA protein

Evolutionary Trace (ET) analysis was applied to the 27 prioritized variants, assigning a ranked variability score (rvET) to each residue. Lower rvET scores indicate a higher degree of evolutionary conservation (Table 1).

Table 1. Evolutionary trace (ET) analysis of HEXA missense variants and their corresponding rvET scores

Variant	Residue	rvET score
c. 340G>A	p. Glu114Lys	4.07
c. 380T>G	p. Leu127Arg	35.73
c.509 G>A	p. Arg170Gln	2.07
c. 508C>T	p.Arg170Trp	2.07
c. 533G>A	p. Arg178His	3.64
c. 532C>T	p. Arg178Cys	3.64
c. 536A>G	p. His179Arg	19.93
c. 590A>C	p. Lys197Thr	6.39
c. 607T>G	p. Trp203Gly	15.29
c. 637T>C	p. Tyr213His	49.48
c. 736G>A	p. Ala246Thr	19.66
c. 749G>A	p. Gly250Asp	7.15
c. 755G>A	p. Arg252His	24.5
c. 754C>T	p. Arg252Cys	24.5
c. 772G>C	p. Asp258His	4.4
c. 805G>C	p. Gly269Arg	27.13
c. 964G>A	p. Asp322Asn	1.39
c. 965A>T	p. Asp322Val	1.39
c. 1260G>C	p. Trp420Cys	27.11
c. 1360G>A	p. Gly454Ser	10.48
c. 1385A>T	p. Glu462Val	8.16
c. 1422G>C	p. Trp474Cys	13.93
c. 1444G>A	p. Glu482Lys	7.12
c. 1496G>A	p. Arg499His	11.11
c. 1495C>T	p. Arg499Cys	11.11
c.1511 G>A	p. Arg504His	37.21
c.1510 C>T	p. Arg504Cys	37.21

Identification of common HEXA variants

Based on published studies describing founder mutations in populations with a high prevalence of Tay–Sachs disease, two missense variants were identified: p.Gly269Ser in the Ashkenazi Jewish population and p.Arg170Trp in the French-Canadian population, as reported by Monaghan et al. and Sillon et al., respectively (20,21). Only p.Arg170Trp (R170W) satisfied the filtering criteria and was selected for further analyses (Figure 1, Table 2).

Secondary and tertiary structure of the R170W variant

PSIPRED analysis of the French-Canadian missense variant revealed the replacement of a positively charged, polar arginine with a bulky, hydrophobic tryptophan, which alters the physicochemical properties of this region. Despite the structural stability and conserved sequence pattern, this amino acid replacement induces a localized transition of the secondary structure from a β-strand to a coil conformation near the mutation site. Overall, this variant induces a localized structural/functional disturbance that can impair normal protein function through reduced local rigidity and altered physicochemical properties of the affected region (Figure 6).

[DOI: 10.29252/JCBR.X.X.X]

Table 2. List of HEXA pathogenic variants that are more frequent in high-prevalence populations

Variant	Protein change	Type of mutation	Population	Source of information
1278insTATC	---	Frameshift	Ashkenazi Jewish	(21)
c.1421+1G>C	---	Splicing	Ashkenazi Jewish	(21)
c. 805G>A	p. Gly269Ser	Missense	Ashkenazi Jewish	(21)
c.805+1G>A (IVS7+1G>A)	---	Splice-site mutation	French-Canadian	(20)
c.508C>T	p. Arg170Trp	Missense	French-Canadian	(20)
c.237_253+7del	---	Frameshift	French-Canadian	(20)
c.1274_1277dup (1278insTATC)	p. Tyr427Ilefs	Frameshif	French-Canadian	(20)
c.−2564_253+5128delinsG (7.6 kb deletion)	---	Large deletion	French-Canadian	(20)
c. 508C>T	p. Arg170Trp	Missense	French-Canadian	(20)
IVS9+1G>A	---	Splice-site mutation	Irish	(34)
1278insTATC	---	Frameshift	Cajun	(35)
c.1073 +1 G>A	---	Splice-site mutation	Cajun	(35)

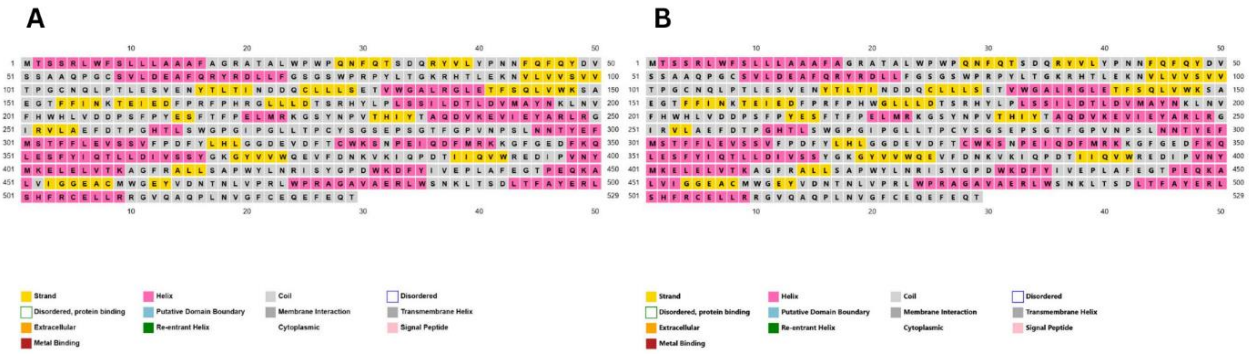


Figure 6. The 2D structure of the missense variant was obtained using PSIPRED. A: wild type; B: French-Canadian missense variant, highlighting the localized secondary-structure perturbation and transition from β-strand to coil conformation in the region surrounding residue 170.

I-TASSER modeling produced similar C-scores for the wild-type and mutant structures (0.18 and 0.20, respectively), indicating preservation of the overall fold. Both models showed identical TM-scores (0.74 ± 0.11), suggesting a conserved topological arrangement. The higher estimated RMSD value (7.0 ± 4.1 Å) likely reflects flexible loop regions rather than major architectural changes. Moreover, both models were assigned to the β-N-acetylhexosaminidase enzyme family (EC: 3.2.1.52) based on the predicted Enzyme Commission classification (Cscore EC = 0.665-0.691) and exhibited strong structural similarity with known enzyme analogs (TM-score ≈ 0.927). Both the catalytic active sites (322 and 323) and the main ligand residues (178, 262, 322, 323, 373, 392, 421, 423, 460, and 462) were conserved in both structures. The Gene Ontology results indicated a remarkably similar pattern of molecular functions, biological processes, and cellular components for the two models, with only subtle differences in the scores of some GO terms. Overall, these structural and functional predictions suggest that the R170W variant does not substantially alter the core catalytic fold or active-site geometry, with its impact likely restricted to subtle changes in local stability and dynamics, although the inherent modeling uncertainty of I-TASSER in flexible loop regions should be acknowledged (Figure 7).

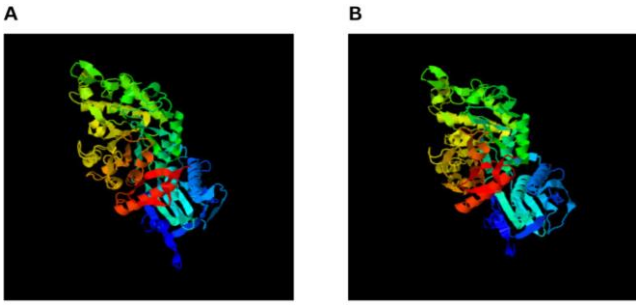


Figure 7. The 3D structure of the HEXA variant compared to the wild type retrieved from I-TASSER. A: The wild type 3D model showed a C-score value of 0.18, indicating a moderate level of prediction confidence; the TM-score (0.74±0.11) suggested a well-conserved global topology, with a relatively high RMSD value of 7.0 ± 4.1 Å.B: The 3D model of the variant showed a C-score value of 0.20 and TM-score and RMSD values identical to those of the wild type.

Hydrophobicity of the R170W variant

ProtScale analysis indicated that substitution of arginine (-4.500) with tryptophan (-0.900) increases local hydrophobicity, potentially affecting conformational stability and molecular interactions.

Stability prediction for the R170W variant

DynaMut2 predicted a destabilizing effect for the R170W substitution, with a ΔΔG value of -1.53 kcal/mol (Figure 8).

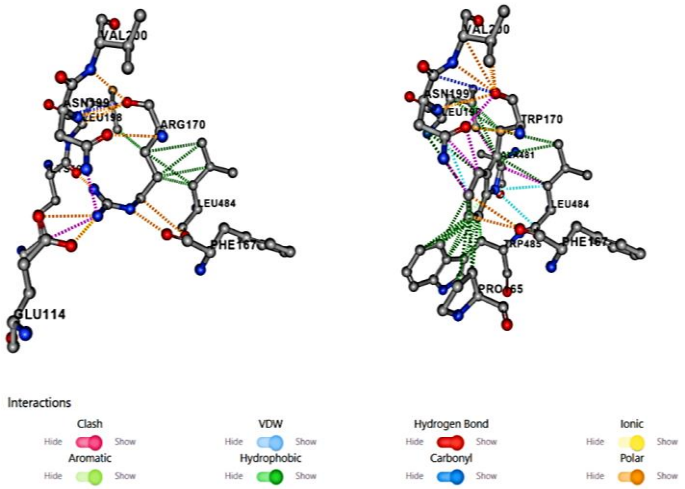


Figure 8. Comparison of intermolecular interactions surrounding residue 170 in the wild-type and mutant HEXA protein. In the wild-type structure, Arg170 participates in ionic and polar interactions that contribute to the stabilization of the local interaction network. Following substitution with tryptophan (R170W), the positively charged arginine residue is replaced by a bulky aromatic side chain, resulting in the loss of ionic interactions and the formation of new aromatic and hydrophobic contacts. In addition, van der Waals clashes are observed in the mutant structure, indicating local structural perturbations. These alterations substantially remodel the interaction network surrounding residue 170 and are consistent with the predicted destabilizing effect of the mutation (ΔΔG = -1.53 kcal/mol), suggesting a reduction in HEXA structural stability and potentially impaired protein function.

[DOI: 10.29252/JCBR.X.X.X]

Discussion

Tay-Sachs disease (TSD) is a progressive neurodegenerative disease caused by a deficiency of the β-hexosaminidase A enzyme. In this study, we systematically evaluated pathogenic missense variants in the HEXA gene through a sequential bioinformatics pipeline to establish a rigorous framework for variant pathogenicity and stability prediction, yielding 27 computationally prioritized candidate variants (22). To evaluate whether our in-silico prioritization aligns with established epidemiological and clinical evidence, we compared these candidates with well-characterized founder mutations reported in high-prevalence populations. This comparison revealed that two historically defined founder variants, c.805G>A [p.Gly269Ser (G269S)] in the Ashkenazi Jewish population and c.508C>T [p.Arg170Trp (R170W)] in the French-Canadian population, were present in the initial variant set (20, 21). After applying pathogenicity consensus filters and thermodynamic destabilization criteria, only p.Arg170Trp met all thresholds and was prioritized for downstream structural and functional characterization, whereas p.Gly269Ser was excluded during the multi-step filtering process. The exclusion of p.Gly269Ser from the final candidate set is also biologically consistent with its established molecular pathology. Clinically, p.Gly269Ser is the canonical allele associated with late-onset Tay–Sachs disease and characteristically retains partial HEXA enzymatic activity (23,24). Consequently, its pathogenic consequence arises primarily from temperature-sensitive protein misfolding and enhanced degradation via the endoplasmic reticulum-associated degradation (ERAD) pathway rather than from a complete loss of enzymatic function. This distinction indicates that founder mutations encompass a wide spectrum of molecular mechanisms and clinical severities. Accordingly, the high population frequency alone does not necessarily reflect severe structural disruption. The retention of p.Arg170Trp throughout all prioritization stages highlights its pronounced structural destabilization alongside its epidemiological prominence, validating its selection for comprehensive biophysical and structural modeling.

A notable finding of this study was that Arg170 is located within the Glycoside Hydrolase Family 20 (GH20) domain, which forms the catalytic core of the β-hexosaminidase A enzyme and is essential for substrate recognition and hydrolysis (25,26). Evolutionary Trace analysis also showed that Arg170 lies within an evolutionarily invariant segment under stringent selective constraints. This finding supports previous evidence demonstrating that many variants associated with infantile Tay-Sachs disease cluster predominantly within conserved functional domains of the HEXA α-subunit (25,27,28). Overall, these findings suggest that Arg170 may play a significant role in preserving the normal structure and function of β-hexosaminidase A.

Structural analyses provided further insight into the potential pathogenic mechanism of this variant. X-ray crystallographic data demonstrate that the hydrogen bond between Arg170 and Glu141 plays an important role in stabilizing the interface between protein domains (29). Consequently, substituting the positively charged, polar arginine residue with a bulky, hydrophobic tryptophan (Trp170) may disrupt this interaction, potentially reducing local structural stability, increasing conformational flexibility, and impairing the efficiency of correct protein folding. Proper folding of the HEXA-encoded α-subunit is essential for functional heterodimerization between the α-subunit and the β-subunit (Encoded by HEXB; Figure 5), suggesting that R170W-induced local instability may impede efficient α/β complex assembly. Structural modeling via I-TASSER revealed that, while the overall fold of the protein remained largely preserved (TM-score > 0.5), local structural fluctuations were evident. The elevated RMSD estimate (7.0 ± 4.1 Å) primarily reflects modeling uncertainties inherent to flexible loop regions rather than global fold collapse. However, static computational predictions cannot fully capture in vivo cellular dynamics; subtle localized perturbations, such as the predicted β-strand-to-coil transition adjacent to residue 170 and the loss of the Arg170-Glu141 interaction, may be biologically amplified under physiological conditions or during lysosomal trafficking. These localized structural perturbations were corroborated by quantitative thermodynamic stability and secondary structure assessments. Thermodynamic profiling via DynaMut2 confirmed a substantial destabilizing impact (ΔΔG = -1.53 kcal/mol), consistent with the consensus predictions from I-Mutant and MUpro. Concurrently, ProtScale profiling demonstrated an elevation in local hydrophobicity upon the introduction of Trp170, while secondary structure predictions via PSIPRED indicated a localized β-strand-to-coil transition adjacent to residue 170. Although this transition does not trigger global unfolding, the combination of increased surface hydrophobicity and thermodynamic destabilization provides a clear trigger for chaperone surveillance. We hypothesize that the exposed nonpolar surface of the misfolded α-subunit promotes aberrant interactions with the endoplasmic reticulum quality control (ERQC) system, potentially channeling it toward the ER-associated degradation (ERAD) pathway, a mechanism previously suggested for several pathogenic HEXA mutations (30). This biophysical cascade explains the severe deficiency of mature lysosomal β-hexosaminidase A in patients harboring the p.Arg170Trp allele.

From a therapeutic standpoint, the preservation of the catalytic machinery combined with susceptibility to ERAD-mediated degradation suggests that R170W may be amenable to pharmacological chaperone therapy (PCT). Small-molecule chaperones may stabilize partially misfolded conformations, facilitating lysosomal trafficking and restoring residual enzyme activity (31-33). Although this principle has been validated in conformational disorders such as phenylketonuria (33), its application in severe infantile Tay-Sachs disease remains constrained by the blood-brain barrier and tight therapeutic windows (32). Thus, structural profiling might prioritize variants amenable to such proteostasis-based precision therapeutics.

Contextualizing our findings with prior in silico studies on HEXA missense variants (e.g., Fazal et al., 2020 (7)) highlights the distinct contributions of this integrated workflow. Previous computational efforts predominantly relied on standalone, sequence-based pathogenicity tools or general evolutionary conservation, often without multi-tiered structural and thermodynamic validation. In contrast, our study provides a more comprehensive, sequential pipeline that integrates consensus pathogenicity filtering (CADD, PolyPhen-2, SIFT, and REVEL) with dual thermodynamic stability assessments (I-Mutant and MUpro), effectively triaging 124 reported pathogenic missense variants down to 27 prioritized candidates. Importantly, our workflow demonstrates how computational thresholds correspond to distinct molecular phenotypes, as illustrated by the algorithmic divergence between p.Arg170Trp and p.Gly269Ser. By performing multiparametric structural characterizations-including thermodynamic destabilization via DynaMut2, local hydrophobicity profiling by ProtScale, secondary-structure transition via PSIPRED, and 3D catalytic site modeling through I-TASSER-our pipeline moves beyond categorical pathogenicity classification to provide a coherent biophysical hypothesis for the R170W founder variant. In accordance with ACMG/AMP variant interpretation guidelines (e.g., criteria PP3 and BP4), these in silico findings serve as rigorous supporting evidence to aid the triage and prioritization of variants of uncertain significance (VUS) for targeted clinical and functional follow-up.

This study also has several limitations. Methodologically, our strict multi-threshold filtering strategy prioritized high-confidence, severe variants to minimize false positives, which inherently risks excluding genuine pathogenic alleles with borderline or discordant algorithmic predictions (Such as p.Gly269Ser). Furthermore, because these findings are derived from computational predictions, they should be assessed as predictive hypotheses requiring empirical confirmation. To bridge the gap between our in-silico findings and clinical phenotypes, we propose a targeted experimental validation roadmap: First, the predicted impact on thermodynamic stability requires experimental validation via biophysical assays, such as circular dichroism (CD) and differential scanning fluorimetry (DSF), to quantify Tm shifts. The involvement of ERAD in the degradation of the misfolded mutant could be assessed by monitoring protein turnover in the presence or absence of proteasome inhibitors such as MG132. Finally, given the structural integrity of the catalytic core, assessing the capacity of pharmacological chaperones to rescue residual enzyme activity in patient-derived fibroblasts remains a critical next step. While molecular dynamics (MD) simulations would provide deeper insights into the conformational dynamics of these variants, the proposed multidisciplinary experimental approach represents a more direct path toward validating our biophysical hypotheses and elucidating the molecular heterogeneity of Tay-Sachs disease.

[DOI: 10.29252/JCBR.X.X.X]

Conclusion

In this study, structural and functional characterization of candidate HEXA missense variants provides valuable insights into the molecular mechanisms underlying Tay-Sachs disease. Our findings suggest that computationally prioritized candidate variants are not necessarily associated with major alterations in the overall protein architecture or catalytic site, but instead may exert their effects through subtle perturbations in protein stability and structural dynamics that are predicted to compromise enzyme function. Collectively, our in-silico analyses indicate that the pathogenic potential of the R170W variant is driven primarily by thermodynamic destabilization and disrupted local interactions, rather than by loss of catalytic site activity. These structural perturbations support a plausible mechanistic hypothesis, suggesting potential folding defects and subsequent ERAD-mediated clearance. Importantly, the computational workflow presented here should be viewed as a variant-prioritization and hypothesis-generating tool, rather than a definitive diagnostic or clinical framework. While this cost-effective strategy successfully triages high-confidence candidate variants, including population-specific founder mutations, computational predictions by themselves cannot replace empirical functional validation, family segregation analysis, or comprehensive clinical interpretation. Ultimately, rigorous experimental and cellular assays are essential before these prioritized variants can be definitively classified or incorporated into diagnostic and carrier screening applications.

Acknowledgement

The authors gratefully acknowledge all individuals who contributed to this work and provided valuable guidance and support throughout the study.

Funding Sources

The present study was financially supported by Golestan University of Medical Sciences (Grant number: 113350).

Ethical Statement

This study received ethical approval from the Ethics Committee of Golestan University of Medical Sciences (Ethics approval code: IR.GOUMS.REC.1401.522).

Conflicts of Interest

The authors declare that they have no conflicts of interest.

Author Contributions

RJK and MH were responsible for the investigation and formal analyses and drafted the initial manuscript. MO contributed to study conceptualization, supervised the project, reviewed and revised the manuscript, validated the methodology, and curated the research data.

Data Availability Statement

No additional data were generated or analyzed beyond those reported in this manuscript.

Use of Artificial Intelligence

AI-based tools were utilized only to assist with language editing. They played no role in data analysis, drafting scientific content, interpreting results, or making scientific decisions.

References

1. Smith JF, Henderson JO. Tay-Sachs Disease: From Molecular Characterization to Ethical Quandaries and the Possibility of Genetic Medicine. J Neurol Res Ther. 2022;4(1):1-13. [View at Publisher] [DOI]
2. Abidi I. Metabolism of Glycosphingolipids and Targeting GM2 Synthesis Pathway to Develop Substrate Reduction Approach in Tay-Sachs and Sandhoff Disorders [thesis]. Kingston (ON): Queen's University (Canada); 2024. [View at Publisher] [Google Scholar]
3. Vasquez KL. Tay-Sachs disease. JNN. 2020;26(6):316-8. [View at Publisher] [DOI] [Google Scholar]
4. González-Sánchez M, Ramírez-Expósito MJ, Martínez-Martos JM. Advances in Diagnosis, Pathological Mechanisms, Clinical Impact, and Future Therapeutic Perspectives in Tay-Sachs Disease. Neurol Int. 2025;17(7):98. [View at Publisher] [DOI] [PMID] [Google Scholar]
5. Vahhab N, Ebrahimi N, Amirmahani F, Vallian S. Analysis of polymorphic markers located in the HEXA gene region associated with Tay-Sachs disease. Meta Gene. 2020:100772. [View at Publisher] [DOI] [Google Scholar]
6. Ibrahim DM, Ali OS, Nasr H, Fateen E, AbdelAleem A. Biochemical and mutational analyses of HEXA in a cohort of Egyptian patients with infantile Tay-Sachs disease. Expansion of the mutation spectrum. Orphanet J Rare Dis. 2023;18(1):52. [View at Publisher] [DOI] [PMID] [Google Scholar]
7. Fazal MI, Kacprzyk R, Timson DJ. In silico analysis of the effects of disease-associated mutations of b-hexosaminidase A in Tay-Sachs disease. J Genet. 2020:99:42. [View at Publisher] [DOI] [Google Scholar]
8. Lewis CJ, Chipman SI, Johnston JM, Acosta MT, Toro C, Tifft CJ. Late-onset GM2 gangliosidosis: magnetic resonance imaging, diffusion tensor imaging, and correlational fiber tractography differentiate Tay-Sachs and Sandhoff diseases. J Neurol. 2025;272(5):355. [View at Publisher] [DOI] [PMID] [Google Scholar]
9. Lew RM, Burnett L, Proos AL, Delatycki MB. Tay-Sachs disease: current perspectives from Australia. Appl Clin Genet. 2015:8:19-25. [View at Publisher] [DOI] [PMID] [Google Scholar]
10. Stenson PD, Mort M, Ball EV, Chapman M, Evans K, Azevedo L, et al. The Human Gene Mutation Database (HGMD®): optimizing its use in a clinical diagnostic or research setting. Hum Genet. 2020;139(10):1197-207. [View at Publisher] [DOI] [PMID] [Google Scholar]
11. Stenson PD, Mort M, Ball EV, Howells K, Phillips AD, Thomas NS, et al. The human gene mutation database: 2008 update. Genome Med. 2009;1(1):13. [View at Publisher] [DOI] [PMID] [Google Scholar]
12. Khajavi M, Inoue K, Lupski JR. Nonsense-mediated mRNA decay modulates clinical outcome of genetic disease. Eur J Hum Genet. 2006;14(10):1074-81. [View at Publisher] [DOI] [PMID] [Google Scholar]
13. Rajavel KS, Neufeld EF. Nonsense-mediated decay of human HEXA mRNA. Mol Cell Biol. 2001;21(16):5512-9. [View at Publisher] [DOI] [PMID] [Google Scholar]
14. Stefl S, Nishi H, Petukh M, Panchenko AR, Alexov E. Molecular mechanisms of disease-causing missense mutations. J Mol Biol. 2013;425(21):3919-36. [View at Publisher] [DOI] [PMID] [Google Scholar]
15. Govindarajan S, Bhaskaran S, Chandrakala B, Muhammadh M. A Review on Tay-Sachs Disease. Eur J Mol Clin Med. 2020;7(3):1681-5. [View at Publisher] [Google Scholar]
16. Leal AF, Benincore-Flórez E, Solano-Galarza D, Garzón Jaramillo RG, Echeverri-Peña OY, Suarez DA, et al. GM2 gangliosidoses: clinical features, pathophysiological aspects, and current therapies. Int J Mol Sci. 2020;21(17):6213. [View at Publisher] [DOI] [PMID] [Google Scholar]
17. Ali MZ, Farid A, Ahmad S, Muzammal M, Mohaini MA, Alsalman AJ, et al. In silico analysis identified putative pathogenic missense nsSNPs in human SLITRK1 gene. Genes (Basel). 2022;13(4):672. [View at Publisher] [DOI] [PMID] [Google Scholar]
18. Ioannidis NM, Rothstein JH, Pejaver V, Middha S, McDonnell SK, Baheti S. REVEL: An ensemble method for predicting the pathogenicity of rare missense variants. Am J Hum Genet. 2016;99(4):877-85. [View at Publisher] [DOI] [PMID] [Google Scholar]
19. Mihalek I, Reš I, Lichtarge O. A family of evolution-entropy hybrid methods for ranking protein residues by importance. J Mol Biol. 2004;336(5):1265-82. [View at Publisher] [DOI] [PMID] [Google Scholar]

[DOI: 10.29252/JCBR.X.X.X]

20. Sillon G, Allard P, Drury S, Rivière J-B, De Bie I. The incidence and carrier frequency of Tay-Sachs disease in the French-Canadian population of Quebec based on retrospective data from 24 years, 1992-2015. J Genet Couns. 2020;29(6):1173-85. [View at Publisher] [DOI] [PMID] [Google Scholar]
21. Monaghan KG, Feldman GL, Palomaki GE, Spector EB, Ashkenazi Jewish Reproductive Screening Working Group, Molecular Subcommittee of the ACMG Laboratory Quality Assurance Committee. Technical standards and guidelines for reproductive screening in the Ashkenazi Jewish population. Genet Med. 2008;10(1):57-72. [View at Publisher] [DOI] [PMID] [Google Scholar]
22. Pejaver V, Byrne AB, Feng B-J, Pagel KA, Mooney SD, Karchin R, et al. Calibration of computational tools for missense variant pathogenicity classification and ClinGen recommendations for PP3/BP4 criteria. Am J Hum Genet. 2022;109(12):2163-77. [View at Publisher] [DOI] [PMID] [Google Scholar]
23. Dersh D, Iwamoto Y, Argon Y. Tay-Sachs disease mutations in HEXA target the α chain of hexosaminidase A to endoplasmic reticulum-associated degradation. Mol Biol Cell. 2016;27(24):3813-27. [View at Publisher] [DOI] [PMID] [Google Scholar]
24. Gravel RA, Triggs-Raine BL, Mahuran DJ. Biochemistry and genetics of Tay-Sachs disease. Can J Neurol Sci. 1991;18(S3):419-23. [View at Publisher] [DOI] [PMID] [Google Scholar]
25. Liu T, Duan Y, Yang Q. Revisiting glycoside hydrolase family 20 β-N-acetyl-D-hexosaminidases: crystal structures, physiological substrates and specific inhibitors. Biotechnol Adv. 2018;36(4):1127-38. [View at Publisher] [DOI] [PMID] [Google Scholar]
26. 26 Val-Cid C, Biarnés X, Faijes M, Planas A. Structural-functional analysis reveals a specific domain organization in family GH20 hexosaminidases. PLoS One. 2015;10(5):e0128075. [View at Publisher] [DOI] [PMID] [Google Scholar]
27. Browne C, Timson DJ. In silico prediction of the effects of mutations in the human mevalonate kinase gene: towards a predictive framework for mevalonate kinase deficiency.Ann Hum Genet. 2015;79(6):451-9. [View at Publisher] [DOI] [PMID] [Google Scholar]
28. Tanaka A, Fujimaru M, Choeh K, Isshiki G. Novel mutations, including the second most common in Japan, in the β-hexosaminidase α subunit gene, and a simple screening of Japanese patients with Tay-Sachs disease. J Hum Genet. 1999;44(2):91-5. [View at Publisher] [DOI] [PMID] [Google Scholar]
29. Lemieux MJ, Mark BL, Cherney MM, Withers SG, Mahuran DJ, James MN. Crystallographic structure of human β-hexosaminidase A: interpretation of Tay-Sachs mutations and loss of GM2 ganglioside hydrolysis. J Mol Biol. 2006;359(4):913-29. [View at Publisher] [DOI] [PMID] [Google Scholar]
30. Mandl Š, Di Geronimo B, Alonso-Gil S, Grininger C, George G, Ferstl U, et al. A new view of missense mutations in α-mannosidosis using molecular dynamics conformational ensembles. Protein Sci. 2025;34(4):e70080. [View at Publisher] [DOI] [PMID] [Google Scholar]
31. Parenti G, Moracci M, Fecarotta S, Andria G. Pharmacological chaperone therapy for lysosomal storage diseases. Future Med Chem. 2014;6(9):1031-45. [View at Publisher] [DOI] [PMID] [Google Scholar]
32. Parenti G, Andria G, Valenzano KJ. Pharmacological Chaperone Therapy: Preclinical Development, Clinical Translation, and Prospects for the Treatment of Lysosomal Storage Disorders. Mol Ther. 2015;23(7):1138-48. [View at Publisher] [DOI] [PMID] [Google Scholar]
33. Pey AL, Ying M, Cremades N, Velazquez-Campoy A, Scherer T, Thöny B, et al. Identification of pharmacological chaperones as potential therapeutic agents to treat phenylketonuria. J Clin Invest. 2008;118(8):2858-67. [View at Publisher] [DOI] [PMID] [Google Scholar]
34. Hernandez M, Tifft C. P192: CRISPR-mediated base editing of the Irish infantile Tay-Sachs mutation. Genet Med Open. 2025;3.35. [View at Publisher] [DOI] [Google Scholar]
35. McDowell GA, Mules EH, Fabacher P, Shapira E, Blitzer MG. The presence of two different infantile Tay-Sachs disease mutations in a Cajun population. Am J Hum Genet. 1992;51(5):1071-7. [View at Publisher] [PMID] [Google Scholar]

Cite this article as:

Jafari Kalokan R, Hajmohammadi M, Oladnabi M. Comprehensive in silico prioritization and functional characterization of pathogenic HEXA missense variants in Tay-Sachs disease. *JCBR.* 2026;X(X):X. http://dx.doi.org/10.29252/JCBR.X.X.X

[DOI: 10.29252/JCBR.X.X.X]

Supplementary Table 1. Prediction of pathogenicity and stability of missense mutations in Tay-Sachs disease (TSD) genes worldwide

Variants	Reported protein effect	ACMG	CADD	SIFT	PolyPhen-2	REVEL	I-Mutant	MUpro	InterPro
c. 340G>A	p. Glu114Lys	Phathogenic	23.9	Deleterious	Probably damaging (1.00)	Deleterious (Moderate) (0.9)	Decrease stability (-0.97)	Decrease stability (-0.89)	N-terminal domain
c. 380T>G	p. Leu127Arg	Phathogenic	26.1	Deleterious	Probably damaging (1.00)	Deleterious (Moderate) (0.91)	Decrease (DDG=-1.62)	Decrease (DDG=-1.62)	N-terminal domain
c.509 G>A	p. Arg170Gln	Phathogenic	28.9	Deleterious	Probably damaging (1.00)	Deleterious (Strong) (0.98)	Decrease (DDG=-1.49)	Decrease (DDG=-0.56)	Catalytic domain
c. 508C>T	p. Arg170Trp	Phathogenic	25.9	Deleterious	Probably damaging (1.00)	Deleterious (Strong) (0.94)	Decrease (DDG=-1.02)	Decrease (DDG=-0.44)	Catalytic domain
c. 533G>A	p. Arg178His	Phathogenic	29.2	Deleterious	Probably damaging (1.00)	Deleterious (Strong) (0.99)	Decrease (DDG=-0.78)	Decrease (DDG=-0.94)	Catalytic domain
c. 532C>T	p. Arg178Cys	Phathogenic	32	Deleterious	Probably damaging (1.00)	Deleterious (Strong) (0.95)	Decrease (DDG=-1.22)	Decrease (DDG=-0.47)	Catalytic domain
c. 536A>G	p. His179Arg	Phathogenic	25.4	Deleterious	Probably damaging (0.999)	Deleterious (Strong) (0.99)	Decrease (DDG=-0.29)	Decrease (DDG=-1.08)	Catalytic domain
c. 590A>C	p. Lys197Thr	Phathogenic	26.5	Deleterious	Probably damaging (1.00)	Deleterious (Strong) (0.99)	Decrease (DDG=-0.67)	Decrease (DDG=-1.05)	Catalytic domain
c. 607T>G	p. Trp203Gly	Phathogenic	28.3	Deleterious	Probably damaging (1.00)	Deleterious (Strong) (0.97)	Decrease (DDG=-3.69)	Decrease (DDG=-2.43)	Catalytic domain
c. 637T>C	p. Tyr213His	Phathogenic	25.8	Deleterious	Probably damaging (1.00)	Deleterious (Moderate) (0.91)	Decrease (DDG=-1.32)	Decrease (DDG=-1.07)	Catalytic domain
c. 736G>A	p. Ala246Thr	Phathogenic	26.1	Deleterious	Probably damaging (1.00)	Deleterious (Strong) (0.95)	Decrease (DDG=-0.65)	Decrease (DDG=-1.06)	Catalytic domain
c. 749G>A	p. Gly250Asp	Phathogenic	26	Deleterious	Probably damaging (1.00)	Deleterious (Strong) (0.94)	Decrease (DDG=-1.77)	Decrease (DDG=-0.59)	Catalytic domain
c. 755G>A	p. Arg252His	Phathogenic	28.2	Deleterious	Probably damaging (1.00)	Deleterious (Strong) (0.96)	Decrease (DDG=-1.41)	Decrease (DDG=-0.74)	Catalytic domain
c. 754C>T	p. Arg252Cys	Phathogenic	29.8	Deleterious	Probably damaging (1.00)	Deleterious (Moderate) (0.89)	Decrease (DDG=-0.85)	Decrease (DDG=-0.38)	Catalytic domain
c. 772G>C	p. Asp258His	Phathogenic	27	Deleterious	Probably damaging (1.00)	Deleterious (Strong) (0.99)	Decrease (DDG=-0.86)	Decrease (DDG=-0.89)	Catalytic domain
c. 805G>C	p. Gly269Arg	Phathogenic	33	Deleterious	Probably damaging (1.00)	Deleterious (Strong) (0.98)	Decrease (DDG=-1.29)	Decrease (DDG=-0.12)	Catalytic domain
c. 964G>A	p. Asp322Asn	Phathogenic	28.3	Deleterious	Probably damaging (0.998)	Deleterious (Moderate) (0.92)	Decrease (DDG=-0.97)	Decrease (DDG=-1.27)	Catalytic domain
c. 965A>T	p. Asp322Val	Phathogenic	27.6	Deleterious	Probably damaging (0.999)	Deleterious (Strong) (0.98)	Decrease (DDG=-0.56)	Decrease (DDG=-0.80)	Catalytic domain
c. 1260G>C	p. Trp420Cys	Phathogenic	27.8	Deleterious	Probably damaging (1.00)	Deleterious (Moderate) (0.88)	Decrease (DDG=-1.75)	Decrease (DDG=-0.69)	Catalytic domain
c. 1360G>A	p. Gly454Ser	Phathogenic	27.4	Deleterious	Probably damaging (1.00)	Deleterious (Strong) (0.98)	Decrease (DDG=-1.05)	Decrease (DDG=-0.98)	Catalytic domain
c. 1385A>T	p. Glu462Val	Phathogenic	27.7	Deleterious	Probably damaging (1.00)	Deleterious (Strong) (0.98)	Decrease (DDG=-0.21)	Decrease (DDG=-0.71)	Catalytic domain
c. 1422G>C	p. Trp474Cys	Phathogenic	33	Deleterious	Probably damaging (1.00)	Deleterious (Strong) (0.96)	Decrease (DDG=-1.25)	Decrease (DDG=-0.54)	Catalytic domain
c. 1444G>A	p. Glu482Lys	Phathogenic	28.9	Deleterious	Probably damaging (1.00)	Deleterious (Strong) (0.95)	Decrease (DDG=-1.20)	Decrease (DDG=-1.15)	Catalytic domain
c. 1496G>A	p. Arg499His	Phathogenic	27.5	Deleterious	Probably damaging (1.00)	Deleterious (Moderate) (0.89)	Decrease (DDG=-1.33)	Decrease (DDG=-1.21)	C-terminal domain
c. 1495C>T	p. Arg499Cys	Phathogenic	31	Deleterious	Probably damaging (1.00)	Deleterious (Moderate) (0.89)	Decrease (DDG=-1.02)	Decrease (DDG=-0.90)	C-terminal domain
c.1511 G>A	p. Arg504His	Phathogenic	29.2	Deleterious	Probably damaging (1.00)	Deleterious (Moderate) (0.9)	Decrease (DDG=-1.59)	Decrease (DDG=-1.2)	C-terminal domain
c.1510 C>T	p. Arg504Cys	Phathogenic	33	Deleterious	Probably damaging (1.00)	Deleterious (Strong) (0.94)	Decrease (DDG=-0.85)	Decrease (DDG=-0.68)	C-terminal domain

[DOI: 10.29252/JCBR.X.X.X]